Generalized transfer matrix theory of electronic transport through a graphene waveguide

Haidong Li,[1] Lin Wang,[1] Zhihuan Lan,[2] and Yisong Zheng[1,*]
[1]*National Laboratory of Superhard Materials, Department of Physics, Jilin University, Changchun 130023, China*
[2]*Department of Aviation Ordnance Engineering, Air Force Aviation University, Changchun 130022, China*
(Received 5 November 2008; published 17 April 2009)

In the effective-mass approximation, electronic property in graphene can be characterized by the relativistic Dirac equation. Within such a continuum model we investigate the electronic transport through graphene waveguides formed by connecting multiple segments of armchair-edged graphene nanoribbons of different widths. By using appropriate wave function connection conditions at the junction interfaces, we generalize the conventional transfer matrix approach to formulate the linear conductance of the graphene waveguide in terms of the structure parameters and the incident electron energy. In comparison with the tight-binding calculation, we find that the generalized transfer matrix method works well in calculating the conductance spectrum of a graphene waveguide even with a complicated structure and relatively large size. The calculated conductance spectrum indicates that the graphene waveguide exhibits a well-defined insulating band around the Dirac point, even though all the constituent ribbon segments are gapless. We attribute the occurrence of the insulating band to the antiresonance effect which is intimately associated with the edge states localized at the shoulder regions of the junctions. Furthermore, such an insulating band can be sensitively shifted by a gate voltage, which suggests a device application of the graphene waveguide as an electric nanoswitch.

DOI: 10.1103/PhysRevB.79.155429 PACS number(s): 84.40.Az, 81.05.Uw, 73.23.−b, 72.10.−d

I. INTRODUCTION

The fabrication of graphene, a graphitic sheet of one-atom thickness, is the first experimental realization of truly two-dimensional crystal.[1] Such a carbon material presents many unusual electronic and transport properties, such as the half-integer quantum Hall effect,[2–6] the nonzero conductivity minimum at vanishing carrier concentration,[5,7–13] the subtle weak localization,[14–19] and the reflectionless transmission of the carrier through an arbitrarily high barrier.[20–22] From the application point of view, graphene has very high mobility and shows am-bipolar behavior.[23] More importantly, the planar geometry of graphene makes it relatively easier to fabricate various integrated nanocircuits. Therefore, graphene is regarded as a perspective base for the postsilicon electronics.

Motivated by possible device applications, electronic transport through various graphene nanostructures was extensively studied both experimentally and theoretically.[24–34] Among these structures, graphene nanoribbon (GNR) is the basic element to carry the current flow. Band-structure calculation indicates that the zigzag-edged GNR is always metallic while the armchair-edged ones are either metallic or semiconducting, depending on their width.[30] Recent experimental work has confirmed the possibility of tunneling the transport gaps of GNRs by changing their widths.[26]

A graphene junction can be formed by interconnecting two semi-infinite GNRs with different widths. In such a graphene nanostructure, a traveling carrier is scattered by the junction interface. Thus, a finite junction conductance appears.[32,33] Furthermore, when connecting multiple distinct graphene fragments (GFs) in cascade manner, one can build up graphene multiple junction (GMJ) structure. It was experimentally demonstrated that the ballistic transport in graphene can be retained over submicron scale.[4] Therefore, the scattering of geometrical shape of a GMJ plays a dominant role in determining its electronic transport property. Recently, the conductance spectrum of a graphene single junction is studied in details.[32,33] It was found that the presence of the lattice vacancy can efficiently enhance the junction conductance,[34] as a vacancy makes the coupling between the electron states of the two GNRs at the junction interface stronger. In contrast, the investigation on electronic transport through GMJs and other graphene waveguides is still in its infancy. However, one can reasonably expect that the graphene waveguides possess many interesting electronic transport properties controlled by their geometrical shapes. For instance, in contrast to a graphene single junction, the GMJ has more junction interfaces. Thus more electron partial waves, including the incident wave and the multiple reflected waves from different interfaces, will take part in the quantum interference. As a result, some transport features observed in graphene single junction can be enhanced or weakened, depending on the details of the geometrical shape of the GMJ. Prior to the experimental realization to fabricate graphene waveguides with high edge-order, theoretical prediction on the geometrical shape dominated electronic transport properties of typical graphene waveguides is highly desirable.

So far two kinds of theoretical approaches, the tight-binding method and the continuum model have been frequently employed to study the electronic and transport properties of graphene bulk material and graphene nanostructure.[35–39] The tight-binding method is suitable to treat the electronic state of graphene nanostructures with arbitrary shapes. Combined with the Landauer-Büttiker formula in discrete lattice representation,[40,41] this method is convenient to study the electronic transport through graphene nanostructures, with various scattering mechanisms included naturally. However, as the size of the graphene nanostructure under consideration increases, the tight-binding method runs into an embarrassment since it needs to treat large matrices. Hence the calculation becomes rather time-consuming. In contrast, such a problem does not occur in the continuum

model which is established based on the effective-mass approximation.[42,43] The continuum model has succeeded in describing the electronic and transport properties of the bulk graphene. When applying it to the nanostructures with relatively large sizes and regular shapes, some appropriate boundary conditions are needed to solve the Dirac equation in this model.

In the present work, we will investigate theoretically the electronic transport through the GMJ structures. Such a graphene waveguide usually has relatively large size. Thus, we will adopt the continuum model in our theoretical treatment. To study the transport properties we known that the transfer matrix approach is well developed to describe the electronic transport through various quantum waveguides made of conventional semiconductor materials.[44–47] However, when we attempt to apply this approach to graphene waveguide, some generalization is necessary since the electron in graphene obeys the relativistic Dirac equation, rather than the Schrödinger equation for the conventional semiconductor materials. This is just the subject of our present work. By using our generalized transfer matrix method, we calculate the conductance spectrum of the GMJs. We find that the GMJs always present a well-defined insulating band around the Dirac point, no matter whether the GNRs in the GMJ are metallic or semiconducting. We analyze that the origin of the appearance of the insulating band is the antiresonance effect produced by the edge states localized at the lateral zigzag edges of the junction interface. Furthermore, we also find the position of the insulating band can be sensitively adjusted by exerting a gate voltage under the GMJ. According to such a feature, we suggest that the GMJ structures can be considered as a device prototype of a nanoswitch.

The rest of this paper is organized as follows: in Sec. II, a self-contained theoretical framework to formulate the linear conductance of the GMJ structures is elucidated, though it is, in fact, a generalization of the conventional transfer matrix method. At first, we establish the relationship between the linear conductance and the scattering matrix in the GMJ. Then we develop the transfer matrix approach to work out the scattering matrix, which is realized by means of the wave function connection condition and boundary condition at the junction interfaces. In Sec. III, the numerical result on the linear conductance spectrum of some typical GMJs is shown. The antiresonance driven insulating band shown in the calculated conductance spectrum is discussed. Finally, the main results are summarized in Sec. IV.

II. THEORY

A. Scattering matrix and linear conductance

The geometry and the honeycomb lattice structure of the GMJ under our consideration are illustrated in Fig. 1. The relevant structure parameters are also explained in the same figure. Obviously, the basic elements consisting of such a GMJ are armchair-edged GFs of different widths. The two semi-infinite ribbons at the left and right sides serve as two leads for electronic transmission. The other finite GFs are in between, constituting the device region where the electronic tunneling is scattered. It was previously shown that the continuum model can describe the electronic property of an infinitely long armchair-edged GNR very well.[30,48] The electronic eigenstate in such a ribbon obeys the following Dirac equation subjected to a certain boundary condition,

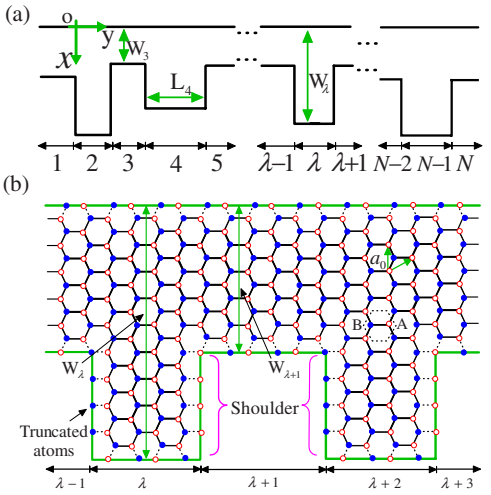

FIG. 1. (Color online) (a) Schematic illustration of a graphene multiple junction structure. (b) The honeycomb lattice of an intermediate part of the graphene multiple junction, around the λth junction. The carbon atoms belonging to the two distinct sublattices, A and B, are distinguishingly labeled as A: ● and B: ○. The atoms at the edges linked to the interior ones by the dashed lines stand for the truncated atoms to shape the GMJ.

$$H\psi = \gamma \begin{bmatrix} 0 & -\hat{k}_- & 0 & 0 \\ -\hat{k}_+ & 0 & 0 & 0 \\ 0 & 0 & 0 & \hat{k}_+ \\ 0 & 0 & \hat{k}_- & 0 \end{bmatrix} \begin{bmatrix} \phi_A \\ \phi_B \\ \phi'_A \\ \phi'_B \end{bmatrix} = E \begin{bmatrix} \phi_A \\ \phi_B \\ \phi'_A \\ \phi'_B \end{bmatrix}, \quad (1)$$

where $\hat{k}_+ = -i\partial_x \pm \partial_y$, $\gamma = \sqrt{3}ta_0/2$ is the so-called Fermi velocity and t being the electron hopping energy between the neighbor lattice points. We choose the Dirac point as the energy reference point and in what follows we use the units $\hbar = t = a_0 = 1$. The electronic eigenstate in the above equation can be analytically solved, which is given by

$$\boldsymbol{u}_{jsk_j}(x,y) = \begin{bmatrix} \phi_A \\ \phi_B \\ \phi'_A \\ \phi'_B \end{bmatrix} = \frac{1}{2\sqrt{W}} \begin{pmatrix} e^{iq_j x} \\ -se^{i\theta_j} e^{iq_j x} \\ -e^{-iq_j x} \\ se^{i\theta_j} e^{-iq_j x} \end{pmatrix} e^{ik_j y}, \quad (2)$$

and the corresponding eigenenergy is $E = s\gamma\sqrt{q_j^2 + k_j^2}$. $s = \pm 1$ denotes the conduction and valence bands, respectively. In Eq. (2) W denotes the width of the ribbon, we have used the lattice constant a_0 as the unit and its length in y direction has been normalized as unity. θ_j is the angle between the wave vector $\boldsymbol{k} = (q_j, k_j)$ and the x axis. The transverse wave vector component q_j takes some discrete values due to the quantum confinement,

$$q_j = \frac{2j\pi}{W} + \frac{2\pi}{3}, \quad j = 0, \pm 1, \pm 2 \cdots . \tag{3}$$

When the ribbon width takes some particular values: $W = 3m/2$ with the integer $m \geq 2$, such a wave vector can be alternatively expressed as $q_j = j\pi/W$. Thus, $q_j = 0$ is allowed, which implies a zero band gap between the conduction and valence bands. In such a particular case the GNR presents a metallic behavior. Herein we need point out that the width W is defined as the distance between the upper and bottom hard walls and scaled in units of the lattice constant a_0, as illustrated in Fig. 1(b). Such a definition is required in our formulation. In previous references the nanoribbon width is measured by the number of the unit cells perpendicular to the armchair edge,[35] equivalently, the number of the carbon atoms along a zigzag line normal to the armchair edge. Of course, the two definitions about the nanoribbon width are equivalent. As we have done, in the formulae we use our definition to denote the width. However, in the next section to show the numerical results, we will use the conventional definition,[49,50] namely, W denotes the number of the unit cells perpendicular to the armchair edge. Thus, whenever $W = 3m' + 2$ with m' being any integer, the nanoribbon is metallic.

In each segment of the GMJ as shown in Fig. 1, the wave function of the electronic state with energy E can be expanded in terms of the eigenstates of the armchair-edged GFs with the same width. To be concrete, such a wave function expansion in λth segment can be expressed as

$$\psi^{\lambda}(x,y) = \sum_j [a_j^{\lambda} u_{jsk_j}^{\lambda} + b_j^{\lambda} u_{js\bar{k}_j}^{\lambda}] + \sum_m [\alpha_m^{\lambda} \tilde{u}_{msp_m}^{\lambda} + \beta_m^{\lambda} \tilde{u}_{ms\bar{p}_m}^{\lambda}], \tag{4}$$

where the wave vector $k_j(p_m) \geq 0$ and $\bar{k}_j(\bar{p}_m) = -k_j(p_m)$. Evidently, the first two terms in the right-hand side of the above equation stand for the propagating modes along the positive and negative directions, respectively. Apart from these propagating modes, we need to add the evanescent modes in the above expansion. The corresponding eigenwave function is given by

$$\tilde{u}_{msp_m} = \begin{pmatrix} e^{iq_m x} \\ -\chi_m e^{iq_m x} \\ -e^{-iq_m x} \\ \chi_m e^{-iq_m x} \end{pmatrix} e^{p_m y}, \tag{5}$$

with

$$\chi_m = s\sqrt{\frac{|q_m + p_m|}{|q_m - p_m|}}\,\mathrm{sgn}(m). \tag{6}$$

Of course, these evanescent modes are unphysical solutions in any uniform ribbon with infinite length. However, they are indispensable in the present GMJ structure to make the wave function continuity at the junction interfaces. Noting that in the left and right leads we should let $\beta^1 = \alpha^{N+1} = 0$ to prevent the wave function from diverging. In Eq. (4) the relation between the wave vectors and the incident electron energy E is

$$E - V = s\gamma\sqrt{q_j^2 + k_j^2} = s\gamma\sqrt{q_m^2 - p_m^2}, \tag{7}$$

where V represents a constant potential to mimic a possible gate voltage exerted in this segment. For a given energy E the number of the propagating mode appearing in the expansion, denoted by J_r^{λ}, is finite and it can be readily determined by the above dispersion relation. On the other hand, one can also see from the above dispersion relation that the number of evanescent modes is in principle infinite. We can actually add an appropriate number of the evanescent modes in the expansion, J_e^{λ}, to guarantee the convergence of the calculated results. Thus the total mode number in λth unit is specified, $J^{\lambda} = J_r^{\lambda} + J_e^{\lambda}$. Such a quantity varies among the segments, depending on their respective widths.

The central task in our theory is to find the scattering matrix which links the injected and the reflected wave amplitudes from the two leads to the device region. Namely,

$$\begin{bmatrix} \boldsymbol{b}^1 \\ \boldsymbol{a}^N \end{bmatrix} = [S] \begin{bmatrix} \boldsymbol{a}^1 \\ \boldsymbol{b}^N \end{bmatrix}. \tag{8}$$

Where $\boldsymbol{a}^1$ and $\boldsymbol{b}^1$ ($\boldsymbol{a}^N$ and $\boldsymbol{b}^N$) are column matrices consisting of the expansion coefficients in Eq. (4), namely, the wave probability amplitudes of all the propagating modes in the left (right) lead. To determine the scattering matrix $[S]$ one should make use of the wave function continuity at all junction interfaces and the formal theory is referred to as the transfer matrix method. But before going into the details about the transfer matrix, we had better to present a brief statement about the relationship between the linear conductance and the scattering matrix, particularly suitable to the GMJ structure.

First of all, we define a pseudo time reversal operator

$$\hat{T} = (\sigma_z \otimes I)\hat{C} = \begin{bmatrix} 0 & 0 & 1 & 0 \\ 0 & 0 & 0 & 1 \\ 1 & 0 & 0 & 0 \\ 0 & 1 & 0 & 0 \end{bmatrix} \hat{C}, \tag{9}$$

with $\hat{C}$ being the complex-conjugate operators. It is commutable with the Dirac Hamiltonian given in Eq. (1). Such a commutation means that in any segment of the GMJ, besides ψ^{λ}, $\hat{T}\psi^{\lambda}$ are also the possible wave function with the same eigenenergy. To be specific, $\hat{T}\psi^1$ and $\hat{T}\psi^N$ are allowable wave functions in the left and right leads. Owing to such an argument the following relation holds true,

$$\begin{bmatrix} \boldsymbol{a}^{1^*} \\ \boldsymbol{b}^{N^*} \end{bmatrix} = [S] \begin{bmatrix} \boldsymbol{b}^{1^*} \\ \boldsymbol{a}^{N^*} \end{bmatrix}. \tag{10}$$

By comparing it with Eq. (8) we find that the scattering matrix satisfies

$$[S]^* = [S]^{-1}. \tag{11}$$

To calculate the probability currents in both leads, we obtain

$$J_L = \langle \Psi^1 | \hat{v}_y | \Psi^1 \rangle = \sum_j [\gamma \sin \theta_j^1 |a_j^1|^2 - \gamma \sin \theta_j^1 |b_j^1|^2], \tag{12}$$

and

$$J_R = \langle \Psi^N | \hat{v}_y | \Psi^N \rangle = \sum_j [\gamma \sin \theta_j^N |a_j^N|^2 - \gamma \sin \theta_j^N |b_j^N|^2]. \tag{13}$$

In the above two equations the velocity operator is defined as $\hat{v}_y = i[H, \hat{y}]$. The probability current conservation requires $J_L = J_R$, namely,

$$\sum_j \sin \theta_j^1 |a_j^1|^2 + \sum_j \sin \theta_j^N |b_j^N|^2 = \sum_j \sin \theta_j^1 |b_j^1|^2 + \sum_j \sin \theta_j^N |a_j^N|^2. \tag{14}$$

If we define a new scattering matrix $[S'] = [v][S][v]^{-1}$ in which the diagonal matrix $[v]$ is defined as $[v] = \text{diag}[\{\sin^{1/2} \theta_j^1\}, \{\sin^{1/2} \theta_j^N\}]$, we can derive from Eq. (14) that the matrix $[S']$ is unitary, namely,

$$[S'][S']^\dagger = 1. \tag{15}$$

From the above relation and Eq. (11) we can deduce the self-transposability $[S']$ matrix,

$$[S'] = [S']^T. \tag{16}$$

Now suppose that an incident electron comes from the lth mode in the left lead. Then it has certain probability to penetrate into the jth mode of the right lead. The corresponding transmission coefficient is defined as the ratio of the incident and the penetrated probability current. By a straightforward calculation we find that such a quantity is associated with the scattering matrix $[S']$. It is given by

$$T_{l \to j} = \frac{J_j}{J_l} = |[S]_{jl}|^2 \frac{\sin \theta_j^N}{\sin \theta_l^1} = |[S']_{jl}|^2. \tag{17}$$

Conversely, for an electron incident from the jth mode in the right lead to enter into the lth mode in the left lead, we can work out the transmission coefficient in the same way,

$$T_{j \to l} = \frac{J_l}{J_j} = |[S]_{lj}|^2 \frac{\sin \theta_l^1}{\sin \theta_j^N} = |[S']_{lj}|^2. \tag{18}$$

The self-transposability of $[S']$ guarantees the symmetry of the transmission coefficients, i.e.,

$$T_{l \to j} = T_{j \to l} = T_{lj}. \tag{19}$$

By virtue of such a relation, when a small bias voltage is established between the left and right leads, the net current can be compactly expressed as

$$I = \frac{e}{h} \int \sum_{jl} T_{jl} [f_R(E) - f_L(E)] dE, \tag{20}$$

where $f_L(E)$ and $f_R(E)$ are the Fermi distribution functions in both leads. Consequently, from the above expression we can readily extract an expression of the linear conductance. It is given by

$$\mathcal{G} = \frac{e^2}{h} \sum_{jl} T_{jl} = \frac{e^2}{h} \sum_{jl} |[S']_{jl}|^2. \tag{21}$$

B. Scattering matrix and transfer matrix

Next we need to work out the scattering matrix with the help of the connection condition of wave functions at the junction interfaces. To illustrate our derivation, we consider the wave function continuity at an arbitrary interface, say the λth one, as shown in Fig. 1(b). It is expressed as

$$\psi_A^\lambda(x, y^\lambda) = \psi_A^{\lambda+1}(x, y^\lambda), \quad 0 \le x < W_{\lambda+1}, \tag{22}$$

and

$$\psi_B^\lambda(x, y'^\lambda) = \psi_B^{\lambda+1}(x, y'^\lambda), \quad 0 \le x < W_{\lambda+1}, \tag{23}$$

where $\psi_A^\lambda(\psi_B^\lambda)$ is a two-component spinor, representing the wave function component belonging to $A(B)$ atoms in λth segment. Noting that $y'^\lambda = y^\lambda - (\sqrt{3})^{-1}$ in the above equations, it arises from the spatial difference between the adjacent A and B atoms. However, such a trivial difference can be safely ignored since in the continuum model which is particularly appropriate to describe the large size structure, the envelope wave function in the preceding equations is slow varying in lattice constant scale. At the shoulder region of the λth junction interface, the wave function component corresponding to the truncated A atoms should vanish. It yields a boundary condition as below

$$\psi_A^\lambda(x, y^\lambda) = 0, \quad W_{\lambda+1} \le x \le W_\lambda. \tag{24}$$

At other junction interfaces there are analogous wave function connection and boundary conditions. From these conditions we can derive a relation about the expansion coefficients in the adjacent segments. First of all, for convenience we adopt the following Dirac notations to denote the respective components of the two sublattices (A and B) in the GF eigenstate. For A atom it is denoted as

$$|\lambda A s^\lambda l k_l^\lambda\rangle = \frac{1}{\sqrt{2W_\lambda}} \begin{pmatrix} e^{iq_l^\lambda x} \\ -e^{-iq_l^\lambda x} \end{pmatrix} e^{ik_l^\lambda y}, \tag{25}$$

and the one for B atom is

$$|\lambda B s^\lambda l k_l^\lambda\rangle = -s^\lambda e^{i\theta_l^\lambda} |\lambda A s^\lambda l k_l^\lambda\rangle. \tag{26}$$

Such a separated expression is equivalent to the eigenwave function given by Eq. (2) except for the trivial change in the normalization constant. For the evanescent modes allowed in the junction structure, the eigenwave function given by Eq. (5) can also be denoted in a separated form,

$$|\lambda A s^\lambda m p_m^\lambda\rangle = \frac{1}{\sqrt{2W_\lambda}} \begin{pmatrix} e^{iq_m^\lambda x} \\ -e^{-iq_m^\lambda x} \end{pmatrix} e^{p_m^\lambda y}, \tag{27}$$

and

$$|\lambda Bs^{\lambda} mp_m^{\lambda}\rangle = -\chi_m |\lambda As^{\lambda} mp_m^{\lambda}\rangle. \tag{28}$$

Noting that to normalize these evanescent eigenmodes is not needed because it does not affect the final form of the scattering matrix. With these notations the wave function connection condition given by Eq. (22) can be rewritten in an expanded form,

$$\begin{aligned}\sum_l [a_l^{\lambda}|\lambda As^{\lambda} lk_l^{\lambda}\rangle + b_l^{\lambda}|\lambda As^{\lambda} l\bar{k}_l^{\lambda}\rangle] + \sum_m [\alpha_m^{\lambda}|\lambda As^{\lambda} mp_m^{\lambda}\rangle \\ + \beta_m^{\lambda}|\lambda As^{\lambda} m\bar{p}_m^{\lambda}\rangle] = \sum_j [a_j^{\lambda+1}|\lambda + 1As^{\lambda+1} jk_j^{\lambda+1}\rangle + b_j^{\lambda+1}|\lambda \\ + 1As^{\lambda+1} j\bar{k}_j^{\lambda+1}\rangle] + \sum_n [\alpha_n^{\lambda+1}|\lambda + 1As^{\lambda+1} np_n^{\lambda+1}\rangle + \beta_n^{\lambda+1}|\lambda \\ + 1As^{\lambda+1} n\bar{p}_n^{\lambda+1}\rangle].\end{aligned} \tag{29}$$

In order to find a relation between these expansion coefficients, we act on the eigenkets in both sides of the above equation by the eigenbra $\langle \lambda As^{\lambda} lk_l^{\lambda}|$. Special attention should be paid to the issue that the integration over x involved in the inner product calculation should be restricted in the narrow region of the junction, namely, $[0, W_{\lambda+1}]$ as labeled in Fig. 1. However, considering the boundary condition given by Eq. (24), such integrations in the left-hand side of Eq. (29) can be safely extended to total interface, i.e., $[0, W_{\lambda}]$. Following such a rule, we obtain

$$\begin{aligned}a_l^{\lambda} + e^{-2ik_l^{\lambda} y^{\lambda}} b_l^{\lambda} = \sum_j [\langle \lambda As^{\lambda} lk_l^{\lambda}|\lambda + 1As^{\lambda+1} jk_j^{\lambda+1}\rangle a_j^{\lambda+1} \\ + \langle \lambda As^{\lambda} lk_l^{\lambda}|\lambda + 1As^{\lambda+1} j\bar{k}_j^{\lambda+1}\rangle b_j^{\lambda+1}] \\ + \sum_n [\langle \lambda As^{\lambda} lk_l^{\lambda}|\lambda + 1As^{\lambda+1} np_n^{\lambda+1}\rangle \alpha_n^{\lambda+1} \\ + \langle \lambda As^{\lambda} lk_l^{\lambda}|\lambda + 1As^{\lambda+1} n\bar{p}_n^{\lambda+1}\rangle \beta_n^{\lambda+1}].\end{aligned} \tag{30}$$

Instead of $\langle \lambda As^{\lambda} lk_l^{\lambda}|$, using the eigenbra $\langle \lambda As^{\lambda} mp_m^{\lambda}|$ to take the inner product we have

$$\begin{aligned}e^{2p_m^{\lambda} y^{\lambda}} \alpha_m^{\lambda} + \beta_m^{\lambda} = \sum_j [\langle \lambda As^{\lambda} mp_m^{\lambda}|\lambda + 1As^{\lambda+1} jk_j^{\lambda+1}\rangle a_j^{\lambda+1} \\ + \langle \lambda As^{\lambda} mp_m^{\lambda}|\lambda + 1As^{\lambda+1} j\bar{k}_j^{\lambda+1}\rangle b_j^{\lambda+1}] \\ + \sum_n [\langle \lambda As^{\lambda} mp_m^{\lambda}|\lambda + 1As^{\lambda+1} np_n^{\lambda+1}\rangle \alpha_n^{\lambda+1} \\ + \langle \lambda As^{\lambda} mp_m^{\lambda}|\lambda + 1As^{\lambda+1} n\bar{p}_n^{\lambda+1}\rangle \beta_n^{\lambda+1}].\end{aligned} \tag{31}$$

The characteristic of the two above equations is that only one specific mode in λth segment (labeling as l or m) is left and the corresponding coefficients are expressed as a function of all the coefficients in $(\lambda+1)$th segment. In addition, if we apply the above procedure to the $(\lambda-1)$th interface, we can obtain two analogous equations:

$$\begin{aligned}a_l^{\lambda} + e^{-2i\theta_l^{\lambda}} e^{-2ik_l^{\lambda} y^{\lambda-1}} b_l^{\lambda} = \sum_j [\langle \lambda Bs^{\lambda} lk_l^{\lambda}|\lambda - 1Bs^{\lambda-1} jk_j^{\lambda-1}\rangle a_j^{\lambda-1} \\ + \langle \lambda Bs^{\lambda} lk_l^{\lambda}|\lambda - 1Bs^{\lambda-1} j\bar{k}_j^{\lambda-1}\rangle b_j^{\lambda-1}] \\ + \sum_n [\langle \lambda Bs^{\lambda} lk_l^{\lambda}|\lambda - 1Bs^{\lambda-1} np_n^{\lambda-1}\rangle \alpha_n^{\lambda-1} \\ + \langle \lambda Bs^{\lambda} lk_l^{\lambda}|\lambda - 1Bs^{\lambda-1} n\bar{p}_n^{\lambda-1}\rangle \beta_n^{\lambda-1}],\end{aligned} \tag{32}$$

and

$$\begin{aligned}\chi_m^2 e^{2p_m^{\lambda} y^{\lambda-1}} \alpha_m^{\lambda} + \beta_m^{\lambda} = \sum_j [\langle \lambda Bs^{\lambda} mp_m^{\lambda}|\lambda - 1Bs^{\lambda-1} jk_j^{\lambda-1}\rangle a_j^{\lambda-1} \\ + \langle \lambda Bs^{\lambda} mp_m^{\lambda}|\lambda - 1Bs^{\lambda-1} j\bar{k}_j^{\lambda-1}\rangle b_j^{\lambda-1}] \\ + \sum_n [\langle \lambda Bs^{\lambda} mp_m^{\lambda}|\lambda - 1Bs^{\lambda-1} np_n^{\lambda-1}\rangle \alpha_n^{\lambda-1} \\ + \langle \lambda Bs^{\lambda} mp_m^{\lambda}|\lambda - 1Bs^{\lambda-1} n\bar{p}_n^{\lambda-1}\rangle \beta_n^{\lambda-1}].\end{aligned} \tag{33}$$

Combining Eqs. (30)–(33) and by a straightforward derivation, it is possible for us to establish an iteration relation between the expansion coefficients of the adjacent segments. It is written in a matrix form as

$$[C^{\lambda}] = [M_{\lambda-1}^{\lambda}][C^{\lambda-1}] + [M_{\lambda+1}^{\lambda}][C^{\lambda+1}], \quad 2 \le \lambda \le N-1, \tag{34}$$

where $[C^{\lambda}]$ is defined as a column matrix consisting of all expansion coefficients in λth segment, namely, $[C^{\lambda}] = [a_1^{\lambda} \cdots a_l^{\lambda} \cdots b_l^{\lambda} \cdots \alpha_m^{\lambda} \cdots \beta_m^{\lambda} \cdots]^T$. The transfer matrices $[M_{\lambda-1}^{\lambda}]$ and $[M_{\lambda+1}^{\lambda}]$ are associated with the inner products appearing in Eqs. (30)–(33). We ignore the details about their definition. But it is not a difficult task to obtain them from the above equations. The feature of the relation given in Eq. (34) is that the coefficient $[C^{\lambda}]$ is expressed explicitly in terms of the two adjacent ones. If we want to work out the next relation, i.e., to express $[C^{\lambda+1}]$ as a function of $[C^{\lambda}]$ and $[C^{\lambda+2}]$, we need to use the above procedure at the $(\lambda+1)$th segment. For example, to establish a relation between $[C^{\lambda+1}]$ and $[C^{\lambda}]$ similar to the ones given in Eqs. (32) and (33), we need to use the connection condition given by Eq. (23).

What we must emphasize herein is that we cannot obtain a simpler transfer matrix to connect two sets of expansion coefficients between the adjacent segments, namely, in the form of $[C^{\lambda}] = [\mathcal{M}_{\lambda+1}^{\lambda}][C^{\lambda+1}]$. This is due to that the numbers of modes in the neighbor segments are different. Instead we can only obtain an iteration relation involving three adjacent segments, as done above. Just due to such an encumbrance, we cannot express $[C^1]$ in terms of $[C^2]$ explicitly. However, by means of the wave function connection conditions at the first junction interface, we can obtain the following relation:

$$[M_1^1][C^1] = [M_2^1][C^2]. \tag{35}$$

Noting that the dimensions of the transfer matrices $[M_1^1]$ and $[M_2^1]$ are, respectively, $J^1 \times 2J^1$, and $J^1 \times 2J^2$. Both are not square matrices. By the same token, at the last junction interface we obtain

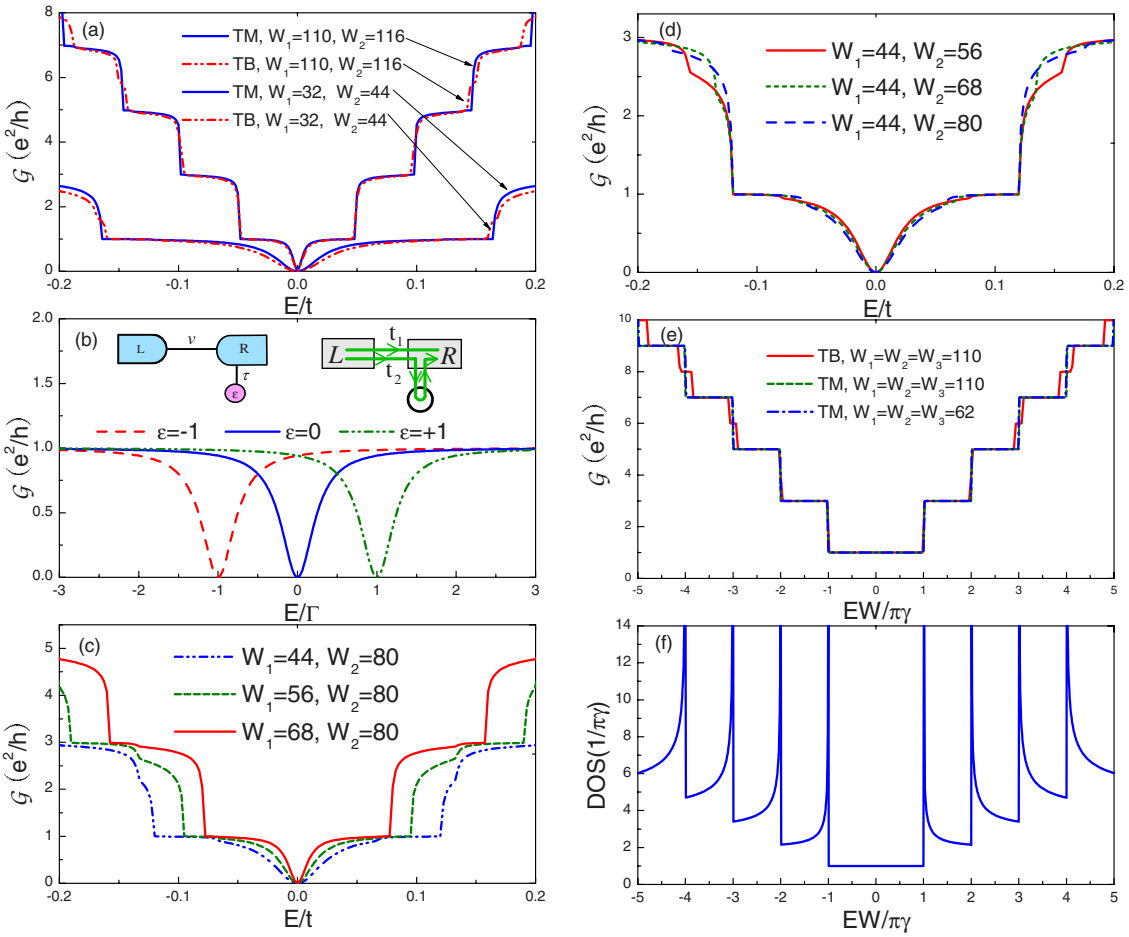

FIG. 2. (Color online) (a) The conductance spectrum of two graphene single junctions with distinct sizes. Comparison is made between the conductance spectra calculated by the tight-binding (TB) and the transfer matrix (TM) methods. (b) Schematic of a laterally coupled quantum dot structure, where v and τ represent, respectively, the coupling coefficients between the two leads and between the quantum dot and the right lead. t_1 and t_2 denote two representative Feynman paths to result in the antiresonance. The calculated conductance spectrum from this model is also plotted. (c) A comparison of the conductance spectra of the graphene single junctions by changing the width of the left lead, whereas the width of the right lead is fixed. (d) Similar to (c), but the width of the right lead is changed with the left lead fixed. [(e) and (f)] The spectra of the conductance and the density of states of GMJ structures as a function of a reduced Fermi energy $EW/\pi\gamma$ when these fragments all have the same width, respectively.

$$[M_N^N][C^N] = [M_{N-1}^N][C^{N-1}]. \tag{36}$$

From the above iteration relations, Eqs. (34)–(36), and by a straightforward derivation we can eliminate all the intermediate coefficients, as well as $[\alpha^1]$ and $[\beta^N]$. As a result, we obtain the scattering matrix $[S]$ defined in Eq. (8).

III. NUMERICAL RESULTS AND DISCUSSIONS

After establishing the transfer matrix theory to describe the electronic transport through the GMJ, we are now in a position to perform the numerical calculation about the conductance spectrum in some typical GMJ structures. Before we proceed, we have to point out that our theory does not involve the electron interaction. This indicates that we consider the transport properties of a spinless electron. All the calculated conductances shown below should be doubled to account for the spin degeneracy. In addition, as mentioned above, the widths W_λ of the GMJ are defined as the number of the carbon atoms along a zigzag line normal to the upper and bottom edges.

At first, we consider a simplest case, a graphene single junction formed by interconnecting the left and right leads directly. We will focus mainly on the electronic transport property in the vicinity of the Dirac point. Therefore, we choose the two leads to be metallic ones which do not present any finite band gap between the conduction and valence bands. In such a case the linear subband across the Dirac point provides a basic channel for the electron transmission through the junction. The calculated conductance spectra ($\mathcal{G}$ vs E) for two single junction structures are shown in Fig. 2(a). We see that the spectrum calculated by our transfer matrix approach agrees well with the one obtained by the tight-binding calculation in the low-energy region. The details about the tight-binding method to calculate the conductance spectrum of a graphene nanostructure can be found in some previous work,[41,51] which is ignored herein to keep the context compact. In particular, for the junction consisting of

relatively wider ribbons the agreement between the results of the two kinds of methods is very satisfactory. Basically, this indicates that our generalization of the transfer matrix method is successful to describe the electron transport through the graphene junction. All these conductance spectra shown in Fig. 2(a) exhibit the staircaselike structures, which can be readily explained by the match of the subband structures of the two metallic leads. The symmetry of the conductance spectra with respect to the Dirac point reflects the subband symmetry between the conduction and valence bands. As the increase of the electron Fermi energy E from the Dirac point, the conductance will jump onto a new staircase at some specific Fermi energies. The appearance of a new step implies that a new transmitting mode is allowed below the Fermi level E. The conductance is proportional to the total number of the allowed modes, which is equal to the subband number of the narrower lead below the Fermi energy. This can be further verified by the results shown in Fig. 2(d). At each step (except for the one near the Dirac point, which will be discussed below), the conductance increases by $2e^2/\hbar$. This is due to the duplicate degeneracy of the subbands except for the lowest linear subband.[30]

An interesting point to note in Fig. 2(a) is that the conductance spectrum shows a notable suppression in the vicinity of the Dirac energy. In particular, a zero conductance occurs at the Dirac energy. At first sight, such a conductance suppression is inconsistent with the gapless subband structure of the two metallic leads. The linear subbands of the two metallic leads always match each other to provide an electron transmission mode. As a result, one can expect that a nonzero conductance appears at the Dirac point. But such a reasoning is dramatically in contradiction with the calculated zero conductance. In fact, the nature of the conductance suppression is the antiresonance effect, which we can explain as follows. In the vicinity of the Dirac energy, only the linear subbands are relevant to the electron transmission. Hence the two metallic GNRs can be viewed as single mode quantum wires coupling to each other directly. However, the zigzag-edged shoulder induces a localized edge state with the eigenenergy equal to the Dirac energy. Such a localized state couples to the linear subband of the wider GNR. Consequently, when the electronic transport is limited in the vicinity of the Dirac point, the graphene junction is equivalent to the T-shaped quantum dot structure as shown in Fig. 2(b). The linear conductance of such a model has been extensively studied,[52–54] which can be expressed in terms of the relevant parameters

$$\mathcal{G}(E) = \frac{e^2}{h}T(E) = \frac{e^2}{h}\frac{4\xi}{(1+\xi)^2}\frac{[E-\varepsilon]^2}{(E-\varepsilon)^2 + \left[\frac{\Gamma}{(1+\xi)}\right]^2}, \tag{37}$$

where $\Gamma = \pi\rho_2\tau^2$ and $\xi = \pi^2\rho_1\rho_2\upsilon^2$ with $\rho_{1(2)}$ being the electron density of the states in two leads. This expression presents a zero conductance at the quantum dot level ε indeed, which is called the antiresonance effect. The antiresonance is in fact a destructive quantum interference. The lateral quantum dot introduces new Feynman paths with a phase shift π. As a result, the destructive quantum interference occurs among electron Feynman paths. We illustrate the quantum interference picture briefly in the following way. From Eq. (37) we find that the conductance $\mathcal{G}(E) \propto |t_1+t_2|^2$ where $t_1 = \sqrt{\pi\rho_1}\upsilon\sqrt{\pi\rho_2}$ and $t_2 = \sqrt{\pi\rho_1}\upsilon\sqrt{\pi\rho_2}(-i)\sqrt{\pi\rho_2}g_2(1+\xi)^{-1}\tau^2\sqrt{\pi\rho_2}$ with $g_2 = [(E-\varepsilon)+i\Gamma(1+\xi)^{-1}]^{-1}$ being the Green's function of the lateral quantum dot. It is reasonable to view t_1 and t_2 as two kinds of different Feynman paths, as illustrated in the inset of Fig. 2(b), where we can see that the path t_2 passes through the lateral quantum dot but t_1 does not. We can readily find that $t_1+t_2=0$ at $E=\varepsilon$. This indicates the completely destructive interference at such an energy. More detailed analysis about the quantum interference picture in terms of the Feynman paths can be found in our previous work.[53] In the metallic graphene junction, the edge state attached to the zigzag-edged shoulder of the junction plays the role of the laterally coupled quantum dot, which results in the antiresonance at the Dirac point. In Fig. 2(c) we calculate several conductance spectra when the width of the narrower lead approaches the wider one whose width is fixed. We find that the suppressed conductance valley becomes narrower as the widths of the two leads approach each other. This effect can be explained in terms of the above quantum dot model. One can readily infer that the parameters υ (the coupling between the two leads) becomes larger, but τ (the coupling between the propagating mode in the wider lead and the edge state localized at the junction shoulder) becomes smaller, as the two leads approach each other in their widths. Consequently, from Eq. (37) one can deduce that the conductance valley becomes narrower. On the contrary, when we fix the width of the narrower lead, but to increase the width of the wider lead, we can see from Fig. 2(d) that conductance valley does not vary notably. This is because that in such a situation the parameter τ, which mainly controls the valley width, does not vary notably as the wider lead is further widened. Besides, the step positions of these different conductance spectra almost appear at the same point. This indicates that the number of transmitting mode to contribute to the conductance is determined by the number of the subbands of the narrower lead under the Fermi energy.

To further check the validity of our transfer matrix theory, we use this approach to calculate the conductance spectra of a single- and a double-junction GMJs in a special case that the widths of all segments are set to take the same value. If our theory is correct, the calculated conductance spectrum should coincide with the one of a graphene nanoribbon with uniform width. In Fig. 2(e) these calculated spectra are shown as a function of a reduced Fermi energy $EW/\pi\gamma$. We can see that these spectra calculated by our transfer matrix theory agree with the tight-binding result of a uniform nanoribbon, which was previously reported.[35] Then, the staircase structure of these spectra originates from the subband structure of the uniform nanoribbon. Scaled by the reduced Fermi energy $EW/\pi\gamma$, the steps of the different spectra appear at the same positions, regardless of the width of the nanoribbon. This can be readily understood, noting that according to the Dirac equation solution the subband bottoms appear at $E_j^{\min} = s\gamma j\pi/W$, namely, scaled by the reduced Fermi energy, the step positions appear at $\pm j$ with $j=0,1,2\ldots$. The conductance jumps by $2e^2/h$ at a step reflects the duplicate de-

generacy of the subbands. This is a result of Dirac equation approach.[30] From tight-binding model this degeneracy is left, which becomes notable for the higher subbands. From the dispersion relation of the subbands given in the above section, we can readily derive the density of states of a uniform nanoribbon. In Fig. 2(f), the density of states of the uniform nanoribbons are shown, which reflects the subband structure and is helpful to account for the staircase structure of the conductance spectra shown in Fig. 2(e).

In Fig. 3(a) we show the calculated conductance spectrum for a step-shaped GMJ. We take the case of $N=3$, namely, a two-junction structure, slightly more complicated than a graphene single junction. First, we can see that the results calculated by the tight-binding and transfer matrix methods, respectively, agree with each other very well. But the tight-binding calculation is much more time-consuming than the corresponding calculation via the transfer matrix method. Second, we can see that the conductance valley around the Dirac point found in a graphene single junction remains and it is further broadened. In Fig. 3(b), the width of the right lead (the wider one) is fixed, the calculated spectrum shows that the conductance valley gets narrower as the two shoulders becomes shorter. In contrast, if we fix the width of the left lead, meanwhile, to increase the width of the two shoulders, the conductance valley is almost invariable. Such a case is shown in Fig. 3(c). These results shown in Figs. 3(b) and 3(c) are consistent with the size dependence of the graphene single junction, as shown in Figs. 2(c) and 2(d). This indicates that the conductance characteristic in a single junction is preserved and further strengthened in the two-junction structures. The results of the conductance spectra shown in Fig. 3(d) indicate that the profile of the steep conductance valley does not vary sensitively with the increase of the longitudinal size of the intermediate ribbon segment. This reflects that the interaction between the two edge states at the two adjacent shoulders is very weak.

The conductance spectra for more complicated step-shaped and T-shaped GMJs are shown in Figs. 4(a) and 4(b), respectively. A common feature of these spectra is that the conductance valley gets steeper as the number of the junctions increases. As shown in Figs. 4(a) and 4(b), when $N>3$ the profile of the conductance valley becomes stable, insensitive to the further increase in the number of the junctions in the structures. This indicates that the conductance valley in a single junction develops rapidly into a well-defined insulating band in the GMJs. Following the antiresonance mechanism mentioned above, it is not very difficult to understand the appearance of the well-defined insulating band in the GMJ. As claimed above, the graphene single junction in the low-energy electron transport regime is equivalent to a lateral quantum dot structure. In an analogous way a mapping between the GMJ and a laterally coupled quantum dot chain, which is illustrated in Fig. 4(c), is reasonable. Of course, the edge states localized at the individual shoulders of the junction interfaces play the roles of the dangling quantum dots and the quantum dots in the main chain mimic the electron states in the ribbon segments. Each quantum dot pair, made of the quantum dot in the main chain and its lateral attachment, can be viewed as an antiresonance unit which contributes a transmission probability amplitude, the

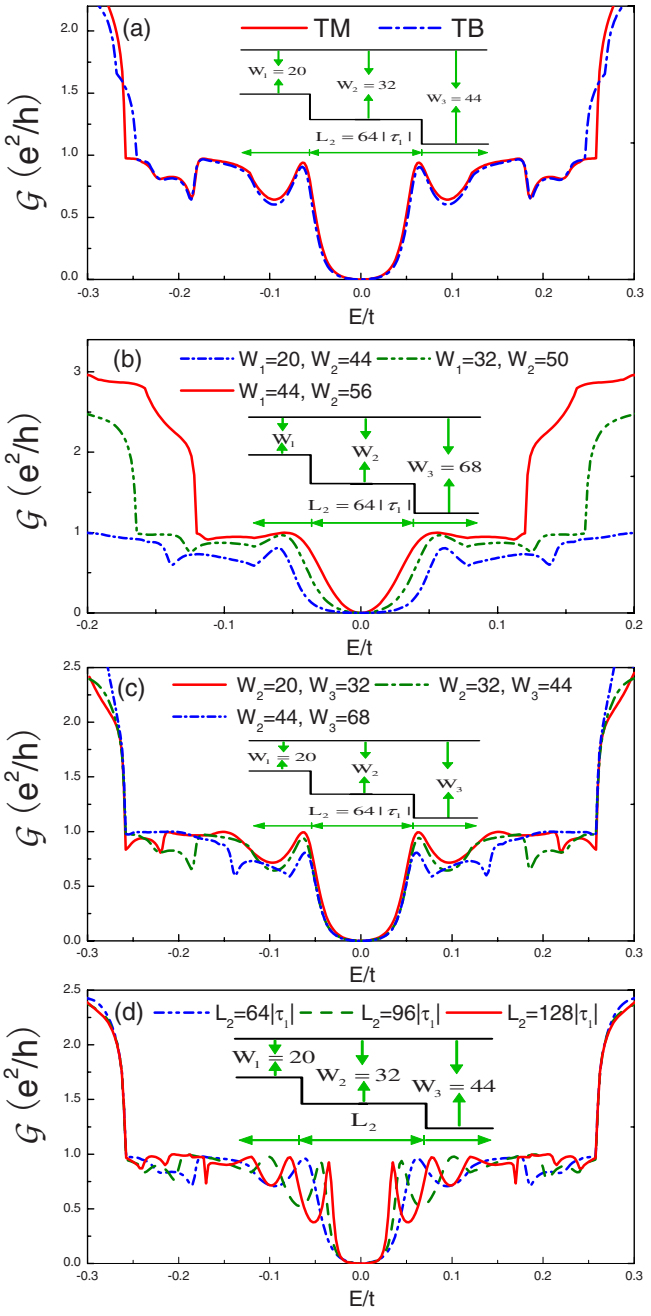

FIG. 3. (Color online) Conductance spectrum of step-shaped two-junction structures (GMJs of $N=3$), $|\tau_1|=\sqrt{3}/3$. (a) A comparison of the calculated results by the tight-binding and the transfer matrix methods. [(b) and (c)] A comparison of the conductance spectrum by changing the width of the junction shoulders. The two different cases with the width of the left and right leads fixed, respectively, are shown in (b) and (c). (d) A comparison of the conductance spectrum by changing the longitudinal size L_2 of the intermediate segment.

squared modulus of which has the same form as the transmission probability given by Eq. (37). In the GMJ the electron wave will be reflected many times by the multiple interfaces before it finally enters into the right leads. The shortest transmission path is the one that the electron penetrates all the junctions directly without any reflection. Even in such a

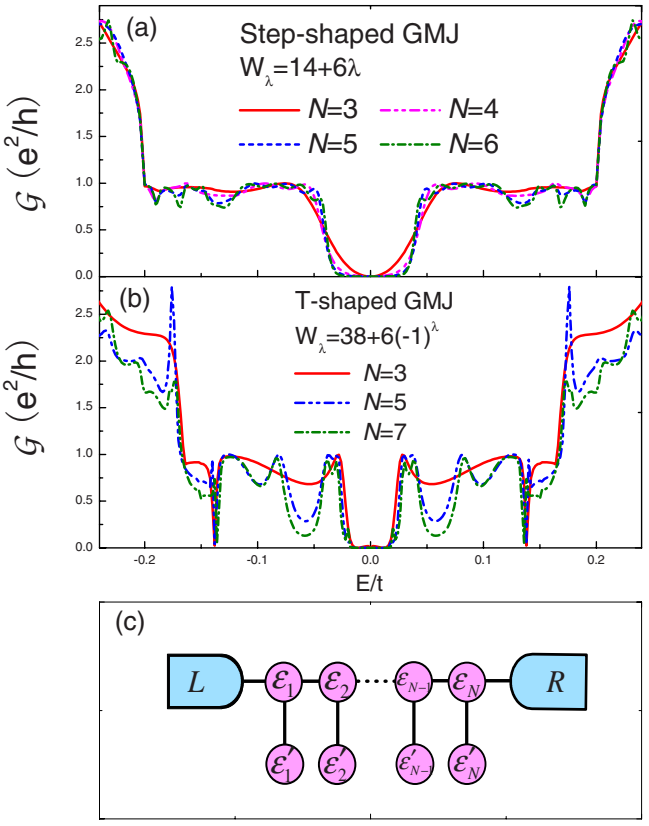

FIG. 4. (Color online) Conductance spectrum of typical GMJ structures. The length of the intermediate ribbon segment is $L_\lambda = 48/\sqrt{3}$. (a) The result of the step-shaped structures. (b) The result of the T-shaped structures. (c) An illustration of the laterally coupled quantum dot chain, which is used to account for the insulating band in the conductance spectrum of the GMJ.

situation, the electron will undergo N junctions, in other words, N antiresonance units. Accordingly, the corresponding transmission probability is proportional to the Nth power of $T(E)$, i.e., $T(E)^N$ [$T(E)$ is the transmission probability of an individual antiresonance unit given by Eq. (37)]. Thus the conductance suppression around the Dirac point included in $T(\omega)$ of each quantum dot is efficiently strengthened. As a result, the antiresonant valley in a single junction evolves into a well-defined insulating band in a GMJ due to multiple quantum interference. A comprehensive explanation about the occurrence of the insulating band in a lateral quantum dot chain was presented in the language of Feynman path in our previous work,[54,55] which can be reasonably used to account for the well-defined insulating band in the present GMJ structures.

In Fig. 5 we show the conductance spectrum which is adjusted by applying a gate voltage under some junctions interfaces. In our theoretical treatment, the gate voltage is mimicked by introducing a finite potential constant in the ribbon segment where the gate voltage is applied. We can see that the insulating band is effectively broadened when certain of the junction interfaces are covered by the gate voltage. But the cost of such a broadening is that the insulating band is not so well defined than the one in the absence of a gate voltage. Such a result can be readily understood according to

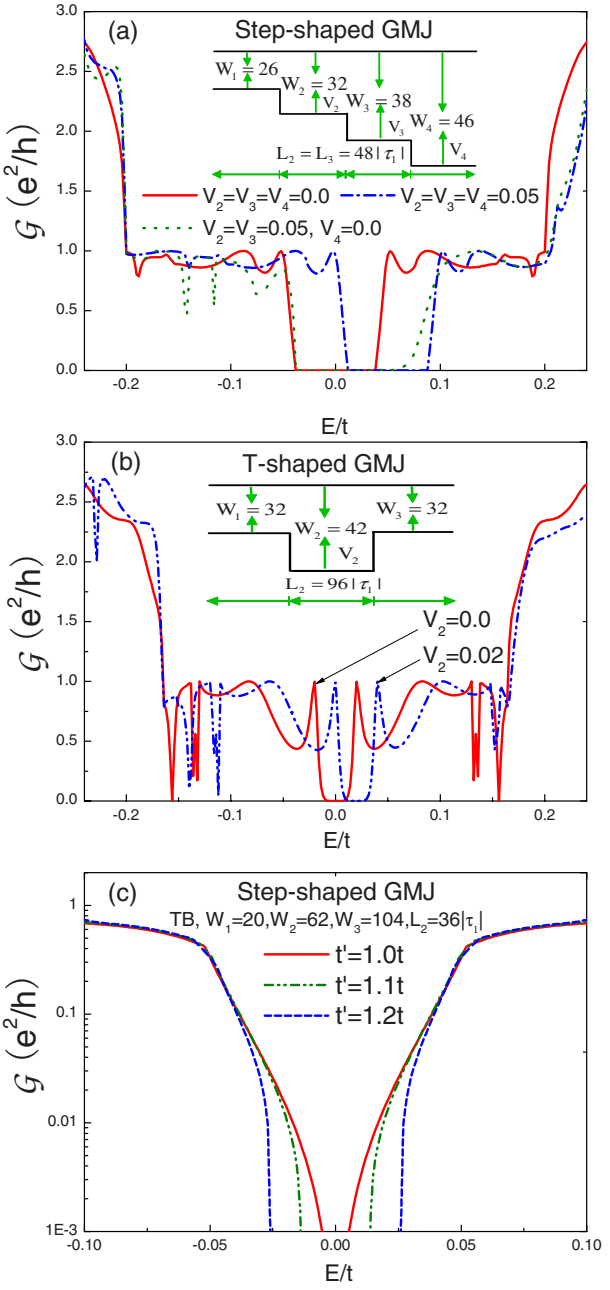

FIG. 5. (Color online) Conductance spectrum of GMJ structures in the presence of the gate voltage. (a) The result of the step-shaped structures. (b) The result of the T-shaped structures. V_λ denotes the potential constant produced by the gate voltage in the λ segment. (c) Conductance spectrum of step-shaped two-junction structures (GMJs of $N=3$), calculated by the modified tight-binding method. t' represents the modified hopping energy of the C-C bonds at the armchair edges.

the multiple quantum interference picture explained above. The transmission probability of each junction possesses a valley center around the level of the localized edge state, in other words, the quantum dot level in the corresponding quantum dot chain. In the absence of a gate voltage such a level is just at the Dirac point. On the other hand, in the presence of a gate voltage covering partially some junctions of the total structure, the levels of the edge states of these

junctions, namely, the centers of these antiresonance units, separates from those of other junctions free from the gate voltage. Accordingly, the total transmission probability presents a broadening of the insulating band, due to that the gate voltage destroys the superposition of the antiresonance centers of all antiresonance units. By the same argument, one can readily understand that the insulating band only exhibits a shift without an observable broadening when all junctions are simultaneously tuned by a gate voltage. In light of the sensitive adjustment of a gate voltage on the insulating band, as shown in Fig. 5, we suggest that the GMJ can be considered as a device prototype of a nanoswitch.

It was reported previously that an armchair-edged graphene nanoribbon always has a finite band gap,[49,50,56] even though it satisfies the metallic condition from which the Dirac equation and simple tight-binding methods predict zero band gap. For the metallic nanoribbon the nonzero band gap originates from the variation in C-C bonding energy (t') at the armchair edges of the nanoribbon. But in our theory, we have not included such a band gap for the metallic nanoribbons. We would like to make the following remarks about this issue. First, the band gap of the metallic nanoribbon gets smaller as its width getting larger. Also our theory is suitable to the large size case. Then, the antiresonance effect cannot be eliminated by the band gap caused by the variation in the bonding energy. We calculate the conductance spectrum of a metallic GMJ, by using the modified tight-binding method which includes the modified bonding energy at the armchair edges. The result is shown in Fig. 5(c) from which we can see that antiresonance effect and the band gap contribute to the insulating gap in the conductance spectra simultaneously. For the large size GMJ, the antiresonance effect becomes the main mechanism to produce the insulating band. Third, the main contribution of our work is to generalize the transfer matrix technique to the graphene waveguides described by the Dirac equation. The advantage of this approach over other methods is that it is suitable to large size GMJ and the relevant calculation is very fast. It can be applied to study the transport properties of more complicated GMJs. The insulating gap of the metallic GMJ due to antiresonance effect is only an interesting feature found by our transfer matrix theory. It is possible for one to incorporate the variation in the bonding energy at the armchair edges into the Dirac equation, and then based on our transfer matrix method, the insulating band in the conductance spectrum of the metallic GMJs can be described more accurately. This issue is left for our further study, but elemental theory, namely, our generalization of the transfer matrix technique, has been established herein.

We notice that the electron transport through carbon nanotube junctions was studied previously.[57,58] There are two differences between the carbon nanotube junction and the graphene junction. The first one is boundary conditions. The nanotube junction implies the periodic boundary condition, but the graphene junction is subject to hard-wall boundary condition. Therefore, when the transverse sizes of the junctions are very small, the conductance spectra of the two distinct junctions are expected to be somewhat different from each other. On the other hand, the conductance spectra of the two junctions almost show the same staircase structure when their transverse sizes are sufficiently large, since in such a case the boundary conditions only influence trivially on the electron subband structures. The second difference is that a graphene junction has the exposed zigzag shoulder to produce the localized edge states, which is responsible for the conductance zero at the Dirac point. As for the nanotube junction it is impossible to form an exposed zigzag edge, so the localized states are absent. As a result, there is no conductance suppression in the nanotube junction around the Dirac point.[58,59]

IV. SUMMARY

By generalizing the transfer matrix approach which was established to describe the electron transport through quantum waveguide made of conventional semiconductor materials, we provide an alternative theoretical method to calculate the conductance spectrum of a GMJ, in place of the tight-binding treatment. By comparing the calculated results by the two methods, we find that our generalized transfer matrix method works well in describing the electronic transport properties of the GMJ structure if its size is not very small. In particular, this method is especially suitable to deal with the GMJs with relatively large sizes and many junctions. In such a case, it is much more timesaving to calculate the conductance spectrum by this method than by the tight-binding calculation. Interestingly, with the transfer matrix method, we find that the GMJ exhibits a well-defined insulating band around the Dirac point, which is due to the strengthening of the intrinsic antiresonance effect of a graphene single junction by the multiple quantum interference at many junction interfaces. By virtue of the feature that the insulating band can be sensitively tuned by a gate voltage, we propose to design a nanoswitch based on this GMJ structure. Our generalized transfer matrix method is also suitable to treat the graphene waveguides with various junction shapes, such as the tortuous nanoribbons with distinct bent angles.

We would like to make some remarks on the issue to implement the function of nanoswitch, by means of the tunability of the insulating band of the GMJ by a gate voltage. In fact, such a transport phenomenon also appears in the T-shaped waveguides and the laterally coupled quantum dot chains,[55,60] made of the conventional semiconductor materials. The similar proposal to make a nanoswitch was previously mentioned in these relevant works. However, the occurrence of a well-defined insulating band in these quantum structures requires that the fluctuation of the quantum dot energy levels (the size of the stubs in a T-shaped waveguide) to be sufficiently small. It is indeed a challenging task to fabricate many identical quantum dots and connecting them periodically in a circuit to realize the function of nanoswitch. However, in the present GMJ structures, the problem of energy level fluctuation is automatically avoided since the antiresonant levels are provided by the localized edge state at the zigzag edge, rather than the quantum confinement in the stub region. The energy levels of these localized states are automatically aligned with each other at the Dirac point,

regardless of the details of the shape of the GMJ. This implies the prefect realization of the uniform antiresonance levels. Generally, the insulating band can be easily formed in the step-shaped as well as the T-shaped GMJs. It does not rigidly require the identity of the shapes of every junction. In addition, it is experimentally demonstrated that ballistic transport can be retained in graphene nanostructures over submicron scale. This means that the quantum interference can play a dominant role and even the size of the GMJ becomes very large. Thus the insulating band structure is expected to remain in a GMJ even with a size up to submicron scale. To sum up these features, we can conclude that the GMJs are the optimal candidate as the prototype of the nanoswitch.

ACKNOWLEDGMENTS

This work was financially supported by the National Natural Science Foundation of China under Grant No. NNSFC10774055, the specialized Research Fund for the Doctoral Program of Higher Education (Grant No. SRFDP20070183130), and National Foundation for Fostering Talents of Basic Science (Grant No. J0730311).

*Corresponding author; zys@mail.jlu.edu.cn

[1] K. S. Novoselov, A. K. Geim, S. V. Morozov, D. Jiang, Y. Zhang, S. V. Dubonos, I. V. Grigorieva, and A. A. Firsov, Science **306**, 666 (2004).
[2] Y. Zheng and T. Ando, Phys. Rev. B **65**, 245420 (2002).
[3] V. P. Gusynin and S. G. Sharapov, Phys. Rev. Lett. **95**, 146801 (2005).
[4] Y. Zhang, Y. W. Tan, H. L. Stormer, and P. Kim, Nature (London) **438**, 201 (2005).
[5] K. S. Novoselov, A. K. Geim, S. V. Morozov, D. Jiang, M. I. Katsnelson, I. V. Grigorieva, S. V. Dubonos, and A. A. Firsov, Nature (London) **438**, 197 (2005).
[6] N. M. R. Peres, F. Guinea, and A. H. Castro Neto, Phys. Rev. B **73**, 125411 (2006).
[7] M. I. Katsnelson, Eur. Phys. J. B **51**, 157 (2006).
[8] J. Tworzydlo, B. Trauzettel, M. Titov, A. Rycerz, and C. W. J. Beenakker, Phys. Rev. Lett. **96**, 246802 (2006).
[9] A. K. Geim and K. S. Novoselov, Nature Mater. **6**, 183 (2007).
[10] F. Miao, S. Wijeratne, Y. Zhang, U. C. Coskun, W. Bao, and C. N. Lau, Science **317**, 1530 (2007).
[11] Y. W. Tan, Y. Zhang, K. Bolotin, Y. Zhao, S. Adam, E. H. Hwang, S. Das Sarma, H. L. Stormer, and P. Kim, Phys. Rev. Lett. **99**, 246803 (2007).
[12] K. Ziegler, Phys. Rev. Lett. **97**, 266802 (2006).
[13] K. Ziegler, Phys. Rev. B **75**, 233407 (2007).
[14] H. Suzuura and T. Ando, Phys. Rev. Lett. **89**, 266603 (2002).
[15] S. V. Morozov, K. S. Novoselov, M. I. Katsnelson, F. Schedin, L. A. Ponomarenko, D. Jiang, and A. K. Geim, Phys. Rev. Lett. **97**, 016801 (2006).
[16] A. F. Morpurgo and F. Guinea, Phys. Rev. Lett. **97**, 196804 (2006).
[17] D. V. Khveshchenko, Phys. Rev. Lett. **97**, 036802 (2006).
[18] E. McCann, K. Kechedzhi, V. I. Falko, H. Suzuura, T. Ando, and B. L. Altshuler, Phys. Rev. Lett. **97**, 146805 (2006).
[19] X. Wu, X. Li, Z. Song, C. Berger, and W. A. de Heer, Phys. Rev. Lett. **98**, 136801 (2007).
[20] P. Krekora, Q. Su, and R. Grobe, Phys. Rev. Lett. **92**, 040406 (2004).
[21] M. I. Katsnelson, K. S. Novoselov, and A. K. Geim, Nat. Phys. **2**, 620 (2006).
[22] V. V. Cheianov and V. I. Fal'ko, Phys. Rev. B **74**, 041403(R) (2006).
[23] S. Latil and L. Henrard, Phys. Rev. Lett. **97**, 036803 (2006).
[24] D. A. Areshkin and C. T. White, Nano Lett. **7**, 3253 (2007).
[25] B. Obradovic, R. Kotlyar, F. Heinz, P. Matagne, T. Rakshit, M. D. Giles, M. A. Stettler, and D. E. Nikonov, Appl. Phys. Lett. **88**, 142102 (2006).
[26] M. Y. Han, B. Özyilmaz, Y. Zhang, and P. Kim, Phys. Rev. Lett. **98**, 206805 (2007).
[27] Y. Ouyang, Y. Yoon, J. K. Fodor, and J. Guo, Appl. Phys. Lett. **89**, 203107 (2006).
[28] A. Rycerz, J. Tworzdlo, and C. W. J. Beenakker, Nat. Phys. **3**, 172 (2007).
[29] T. B. Martins, R. H. Miwa, A. J. R. da Silva, and A. Fazzio, Phys. Rev. Lett. **98**, 196803 (2007).
[30] L. Brey and H. A. Fertig, Phys. Rev. B **73**, 235411 (2006).
[31] O. Hod, V. Barone, and G. E. Scuseria, Phys. Rev. B **77**, 035411 (2008).
[32] Z. P. Xu and Q. S. Zheng, Appl. Phys. Lett. **90**, 223115 (2007).
[33] S. Hong, Y. Yoon, and J. Guo, Appl. Phys. Lett. **92**, 083107 (2008).
[34] T. C. Li and S. P. Lu, Phys. Rev. B **77**, 085408 (2008).
[35] N. M. R. Peres, A. H. Castro Neto, and F. Guinea, Phys. Rev. B **73**, 195411 (2006).
[36] V. M. Pereira, J. Nilsson, and A. H. Castro Neto, Phys. Rev. Lett. **99**, 166802 (2007).
[37] J. Q. Lu, J. Wu, W. Duan, F. Liu, B. F. Zhu, and B. L. Gu, Phys. Rev. Lett. **90**, 156601 (2003).
[38] Y. M. Blanter and I. Martin, Phys. Rev. B **76**, 155433 (2007).
[39] L. Brey and H. A. Fertig, Phys. Rev. B **75**, 125434 (2007).
[40] S. Datta, *Electronic Transport in Mesoscopic Systems* (Cambridge University Press, Cambridge, England, 1995).
[41] F. Muñoz-Rojas, D. Jacob, J. Fernández-Rossier, and J. J. Palacios, Phys. Rev. B **74**, 195417 (2006).
[42] T. Ando, J. Phys. Soc. Jpn. **74**, 777 (2005).
[43] D. P. DiVincenzo and E. J. Mele, Phys. Rev. B **29**, 1685 (1984).
[44] A. Weisshaar, J. Lary, S. M. Goodnick, and V. K. Tripathi, J. Appl. Phys. **70**, 355 (1991).
[45] A. Weisshaar, J. Lary, S. M. Goodnick, and V. K. Tripathi, Appl. Phys. Lett. **55**, 2114 (1989).
[46] W. D. Sheng and J. B. Xia, J. Phys.: Condens. Matter **8**, 3635 (1996).
[47] J. B. Xia, Phys. Rev. B **45**, 3593 (1992).
[48] L. Brey and H. A. Fertig, Phys. Rev. B **73**, 195408 (2006).
[49] Y.-W. Son, M. L. Cohen, and S. G. Louie, Phys. Rev. Lett. **97**, 216803 (2006).

[50] L. Yang, C.-H. Park, Y. W. Son, M. L. Cohen, and S. G. Louie, Phys. Rev. Lett. **99**, 186801 (2007).
[51] K. Nakada, M. Fujita, G. Dresselhaus, and M. S. Dresselhaus, Phys. Rev. B **54**, 17954 (1996).
[52] A. Ueda and M. Eto, Phys. Rev. B **73**, 235353 (2006).
[53] Y. Liu, Y. Zheng, W. J. Gong, and T. Lü, Phys. Rev. B **75**, 195316 (2007).
[54] W. J. Gong, Y. Zheng, Y. Liu, and T. Lü, Physica E **40**, 618 (2008).
[55] W. J. Gong, Y. Zheng, Y. Liu, and T. Lü, Phys. Rev. B **73**, 245329 (2006).
[56] H. X. Zheng, Z. F. Wang, T. Luo, Q. W. Shi, and J. Chen, Phys. Rev. B **75**, 165414 (2007).
[57] H. Matsumura and T. Ando, J. Phys. Soc. Jpn. **67**, 3542 (1998).
[58] T. Ando, T. Nakanishi, and R. Saito, J. Phys. Soc. Jpn. **67**, 2857 (1998).
[59] R. Tamura and M. Tsukada, Phys. Rev. B **55**, 4991 (1997).
[60] P. S. Deo and A. M. Jayannavar, Phys. Rev. B **50**, 11629 (1994).